PAPER • OPEN ACCESS

Formation of nanoporous Si upon self-organized growth of Al and Si nanostructures

To cite this article: Annett Thøgersen *et al* 2018 *Nanotechnology* **29** 315602

View the article online for updates and enhancements.

Formation of nanoporous Si upon self-organized growth of Al and Si nanostructures

Annett Thøgersen[1] **, Ingvild J T Jensen**[1]**, Marit Stange**[1]**,
Torunn Kjeldstad**[2]**, Diego Martinez-Martinez**[3]**, Ole Martin Løvvik**[1]**,
Alexander G Ulyashin**[1] **and Spyros Diplas**[1]

[1] SINTEF Materials and Chemistry, PO Box 124 Blindern, NO-0314 Oslo, Norway
[2] Department of Physics, Centre for Materials Science and Nanotechnology, University of Oslo, PO Box
1048 Blindern, NO-0316 Oslo, Norway
[3] Center of Physics, University of Minho, Campus of Azurm, Guimaraes, Portugal

CrossMark

Abstract

Nanostructured materials offer unique electronic and optical properties compared to their bulk
counterparts. The challenging part of the synthesis is to create a balance between the control of
design, size limitations, up-scalability and contamination. In this work we show that self-
organized Al nanowires in amorphous Si can be produced at room temperature by magnetron co-
sputtering using two individual targets. Nanoporous Si, containing nanotunnels with dimensions
within the quantum confinement regime, were then made by selective etching of Al. The material
properties, film growth, and composition of the films were investigated for different
compositions. In addition, the reflectance of the etched film has been measured.

Keywords: nanowires, silicon, self-organization, solar cells, porous silicon, aluminum

(Some figures may appear in colour only in the online journal)

1. Introduction

Porous Si has shown great potential for use in solar cells as
for example as anti-reflection coating. [1] Reducing the
dimensions of Si in one, two, or three directions, creating thin
films, Si nanowires[2] and quantum dots [3], respectively,
introduces quantum confinement effects which increase and
change the bandgap from indirect to direct. [4] This generates
new possibilities for use of Si in optical systems. In addition
to modifying physical properties, the small size does in itself
represent an opportunity for innovation, as it makes sig-
nificantly higher device densities possible for nano-scale
electronics and reduces cost. [5] Nanowire based solar cells,
are attractive for use in solar cell applications due to their
large surface area, anti-reflection properties, high aspect ratio,

and increased charge transport. [5, 6] In addition, Si nano-
wires have also been suggested to be incorporated into
devices such as 1D conductors, [7] energy storage devices,
[8–10] thermoelectric materials, [11] electroluminescent
devices, [12] and nano-scale field-effect transistors. [13]

Nanowires are typically made using either 'top-down'
approaches such as lithography [14] and electroless chemical
etching [15], or 'bottom-up' approaches like adsorbent-
assisted physical vapor deposition, [12] chemical vapor
deposition, [8], colloid assisted epitaxy [16] and electro-
deposition [17]. The 'top-down' approaches offer good con-
trol of the design, but are limited downwards in terms of size,
while the opposite occurs for the 'bottom-up' approaches. A
more unconventional method utilizes the low miscibility
between Al and Si to achieve nanostructures of the two
materials.

In a previous theoretical work, we have shown that for
immiscible elements segregation will tend to occure even
when diffusion is restricted, resulting in the formation of nano
clusters. [18] The maximum solubility of Si in Al is 1.55 at%

at T = 577 °C, while that of Al in Si is as low as 0.001 at% at the same temperature. [19, 20] Phase separation occurs in the form of eutectic morphologies at room temperature upon conventional solidification routes used to produce Si–Al alloys. Al nanowires with diameters of 5–13 nm in an aSi matrix have previously been made by Fukutani *et al* [21], using magnetron sputtering with one silicon–aluminum mixed target, at temperatures between 100 °C–300 °C. Nanoporous silicon films were then made by etching away the Al using a sulfuric acid solution. [22, 23] This nanoporous silicon structure was then used as a template to produce nanowires with other elements, such as Ni [24]. The preference for this phase separation into nanowires has been shown to occur when the compositional ratio is about 50/50 [25], and the formation is strongly affected by the diffusion length [21]. In our work, self-organized Al nanowires in aSi have been made with magnetron sputtering using two targets (Si and Al), performed at room temperature. The versatility of sputtering with two targets makes the composition variations easier to tune. In addition, sputtering at room temperature will help prevent damage and diffusion in the underlying wafer structure, which is crucial if these films are going to be incorporated for example into a solar cell device.

The samples were analyzed using transmission electron microscopy (TEM), x-ray photoelectron spectroscopy (XPS), and UV–vis spectrometry, and then compared to three-dimensional kinetic Monte-Carlo (KMC) simulations. This paper focuses on the fundamental aspects of structure, formation, and composition of these nanoporous structures, while the technological aspect connected to integration in a solar cell device is part of ongoing work.

2. Experimental

Thin films with Al and Si were deposited on mono-crystalline 4 inch Si (100) substrates by a CVC 601 magnetron co-sputtering equipment. Alternating sputtering corresponding to Al and Si layers of about 1 nm were carried out in Ar atmosphere at a working pressure of 3 mTorr, with a power of 400 W for Si and 150 W for Al, with 2.50 rpm and 22 min sputtering time. Homogenous Si–Al films were made by sputtering in an Ar atmosphere at a working pressure of 3 mTorr, with a power of 400 W, from one target consisting of a Si target with Al pieces. The compositional profile was varied between $Si_{0.82}Al_{0.18}$ and $Si_{0.75}Al_{0.25}$ [26]. Cross-sectional TEM samples were selected from several points on the wafer, in order to ensure reproducibility. The samples were prepared by ion-milling using a Gatan precision ion polishing system with 5 kV gun voltage. Plane-view samples were made using Allied High Tech—MultiPrep^{TM} Polishing System with a wedge angle of 2°. The samples were analyzed by high resolution TEM and energy filtered TEM (EFTEM) in a 200 keV JEOL 2010F microscope with a Gatan imaging filter and detector. Scanning TEM (STEM), energy dispersive spectroscopy (EDS), and electron energy loss spectroscopy (EELS) were carried out using a FEI Titan G2 60-300 microscope with a super EDX detector and a Gatan imaging filter. XPS was performed with a

KRATOS AXIS ULTRA^{DLD} using monochromatic Al K$_\alpha$ radiation ($h\nu$ = 1 486.6 eV). The x-ray source was operated at 10 mA and 15 kV. UV–vis$_{NI}$ spectrometry was performed on a Shimadzu UV-1800 spectrometer, with a wavelength range of 190 to 1100 nm.

KMC simulations were carried out using a code programmed according to the method described by Helin *et al* [27] and Tan *et al* [28]. The coating growth is a process which consists of a random vertical ballistic deposition of atoms and subsequent diffusion controlled by atom hopping, using periodic boundary conditions. The atoms are located according to a bi-dimensional square lattice (same number of sites in vertical and horizontal directions), with a compact hexagonal packaging and A-B-A-B stacking of layers in vertical direction. A Morse potential is employed to evaluate the interaction energy between atoms, extended to the next nearest neighbor. The immiscibility is introduced by using a repulsive interaction between elements of different type.

3. Results and Discussion

Si and Al were co-sputtered in thin alternating layers at three different ratios; 70 at% Si/30 at% Al ($Si_{0.7}Al_{0.3}$), 60 at% Si/40 at% Al ($Si_{0.6}Al_{0.4}$), and 30 at% Si/70 at% Al ($Si_{0.3}Al_{0.7}$). The deposition resulted in self-organized Al–Si nanostructures as illustrated in figures 1(IIA), (IIB), and (IIC). In sample $Si_{0.7}Al_{0.3}$ (figure 1(IIA)), Al nanocrystals embedded in aSi were formed. Figure 1(IIA) (bottom) shows a TEM image of the Al nanocrystals, evenly spaced throughout the layer. The spherical nanocrystals have diameters of about 2–3 nm. In sample $Si_{0.6}Al_{0.4}$ (figure 1(IIB)) vertical Al nanowires were formed in the aSi matrix, with a diameter of about 5 nm. Most of the Al nanowires extend from the Si substrate to the surface of the sputtered film in lengths of approximately 100 nm. The nanowires were made on all parts of the Si wafer. Only small variations in Al nanowire quality such as length, thickness and growth angle has been observed. Sample $Si_{0.3}Al_{0.7}$ consists of a mix of larger Al particles, Al nanowires, and nanocrystals (figure 1(IIC)). As presented in a previous paper [26], sputtering with only one composite Si–Al target at room temperature results in an homogenous SiAl film, as presented in figure 1 I. The maximum Al composition tested in these samples were 30 at%, comparable with the sample in figure 1(IIA).

The nanowire growth has been studied preliminary using three-dimensional KMC simulations considering two immiscible elements. As illustrated in figure 2(A), the initial layer of the film corresponds to small islands of the minority element surrounded by the other. Further simulated growth of a film formed by columns embedded in a matrix in conditions of low mobility of adatoms can then be reproduced, as shown in figure 2(B). After the first layer is being deposited, growth of the film adds new layers which follow the structure of the first one, since both elements tend to avoid contact with each other. The formation of nanoparticles instead of columns would be just the consequence of the unbalanced arrival of elements during the deposition, which stops the growth of the
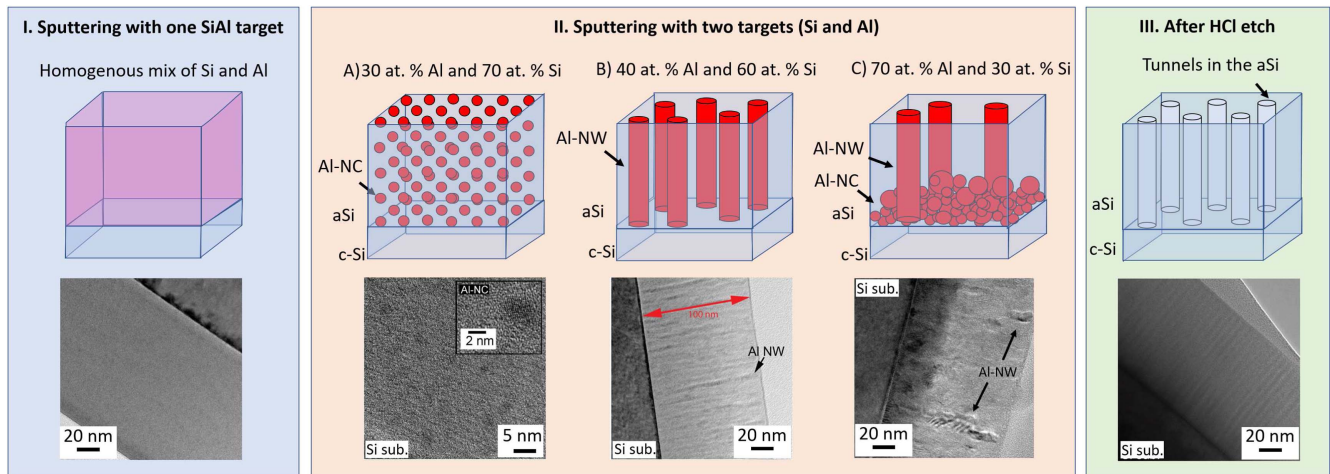
Figure 1. Sketch of the sample structures presented in this paper, with the associated TEM images. (I) Magnetron sputtering with a composite SiAl target. (II) Sputtering with two targets (Si and Al), (IIA) Sample $Si_{0.7}Al_{0.3}$, resulting in Al nanocrystals. (IIB) Sample $Si_{0.6}Al_{0.4}$, resulting in Al nanowires, and (IIC) sample $Si_{0.3}Al_{0.7}$. (III) Sample $Si_{0.6}Al_{0.4}$ after removing the Al nanowires with HCl etching.
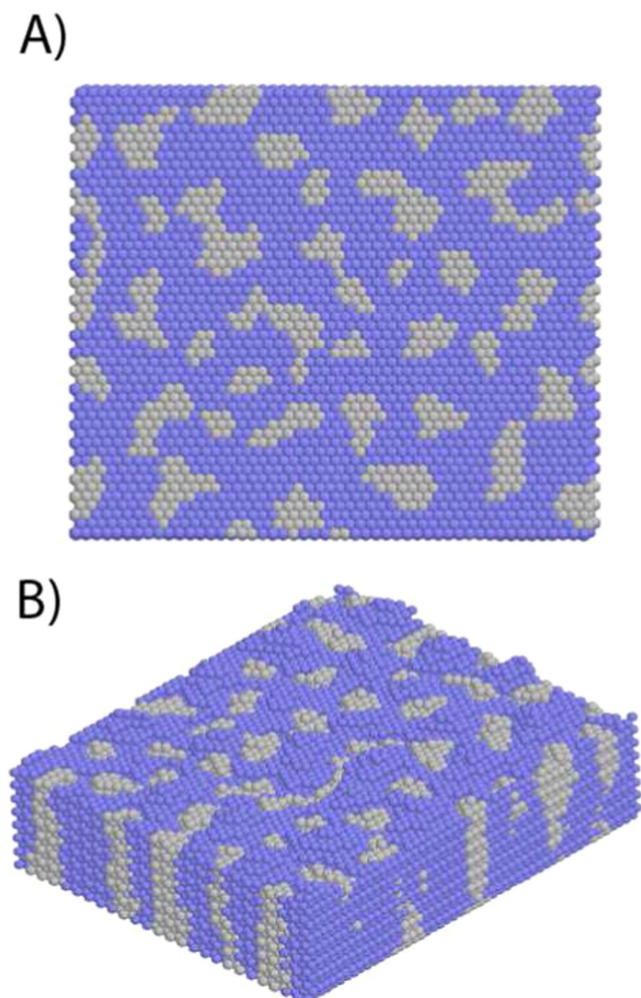

Figure 2. Three-dimensional Kinetic Monte-Carlo simulation of bicomponent immiscible deposition of films in conditions of low adatom mobility and unbalanced chemical composition. (A) First layer of the film, where islands of the minority elements embedded in the second one can be observed. (B) Three-dimensional perspective, where the columnar growth are shown.
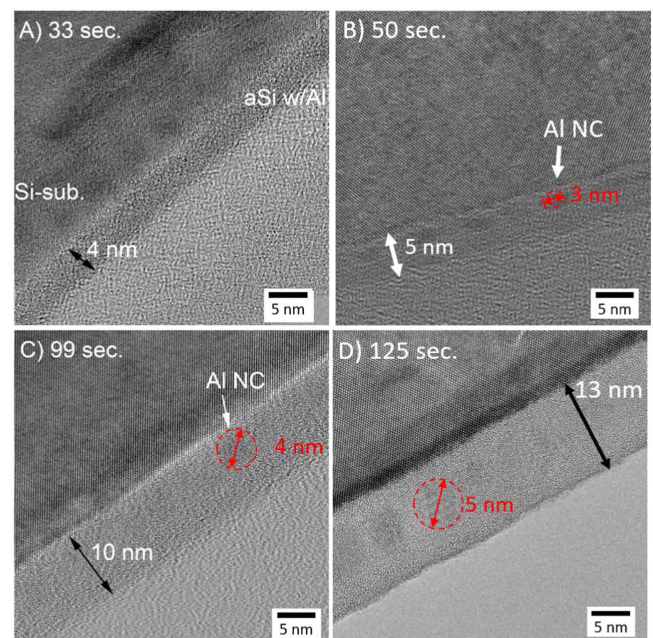
Figure 3. TEM images of the initiation process of Al nanowires after sputtering for (A) 33 s, (B) after 50 s, (C) after 99 s, and (D) after 125 s.

embedded columns by the formation of a continuous layer of the dominant element. It is worth noting that deposition in conditions of large adatom mobility (e.g. larger temperatures) leads to the formation of large agglomerates instead of columns or nanoparticles. This has been observed for the Si–Al system by Fukutani *et al* [23] for temperatures above 300 °C. Other properties of the films, such as low roughness, are also reproduced by the simulations, as it will be described in a forthcoming dedicated publication.
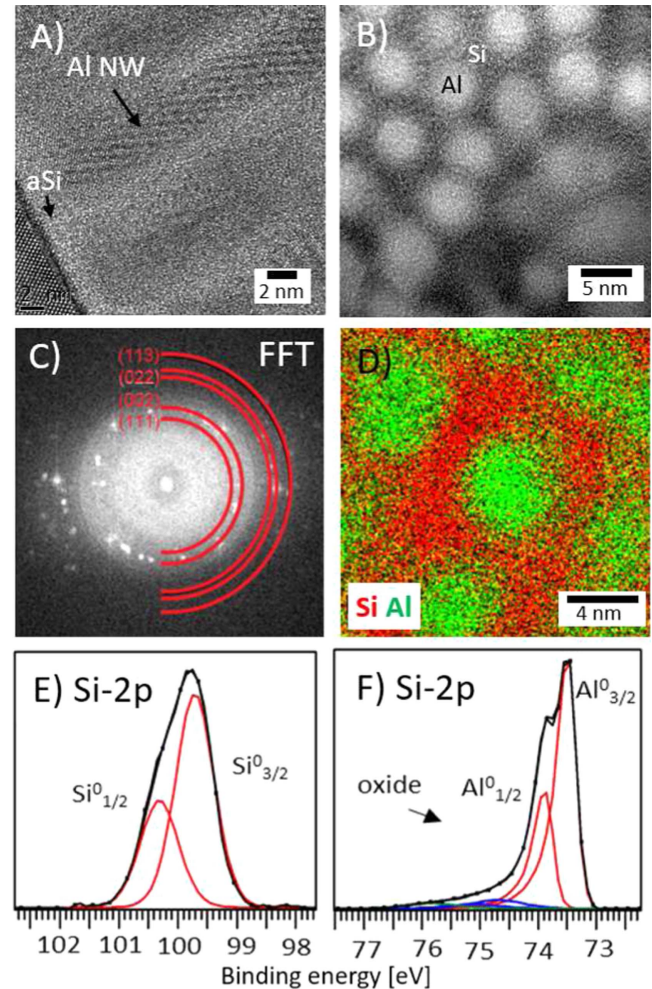
The Monte-Carlo simulations has been confirmed by TEM after depositing for 33 s (figure 3(A)), 50 s (B), 99 s (C), and 125 s (D). After only 33 s, 4 nm of Si–Al has been
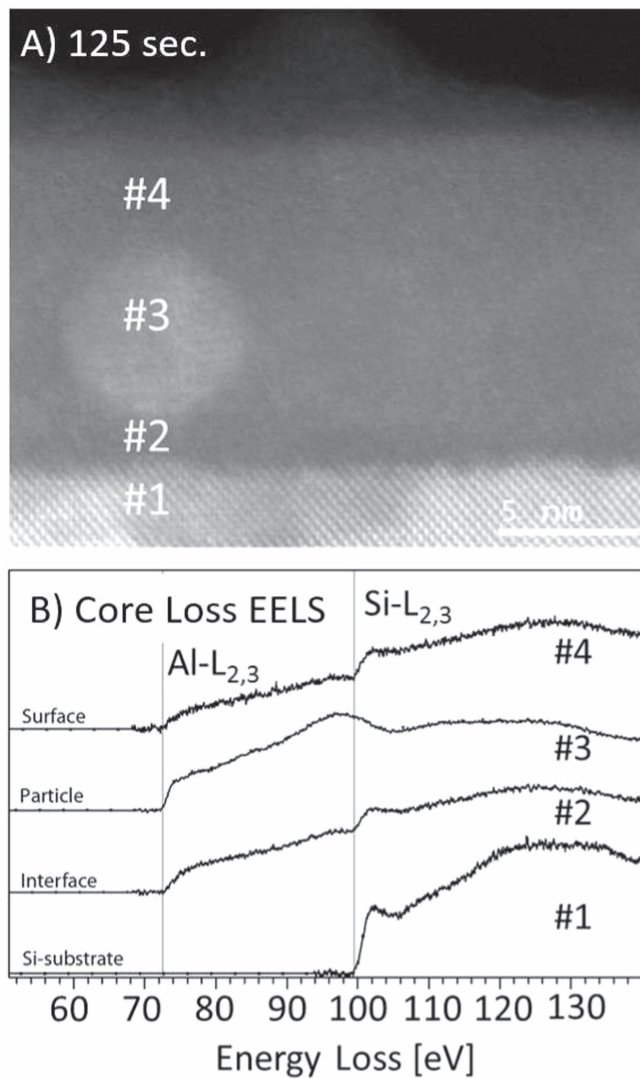
Figure 4. (A) HAADF STEM image of Al nanocrystal made by sputtering for 125 s. (B) EELS core loss spectra of the Al and Si L2, 3 peak, from the STEM image in figure (A).

Figure 5. (A) Cross-sectional image of the nanowires near the substrate in sample $Si_{0.6}Al_{0.4}$. (B) EFTEM image (plane-view) of sample $Si_{0.6}Al_{0.4}$ using the plasmon peak of Al, (C) fast Fourier image of the nanowires in (B). (D) Plane view EDS mapping of Al and Si, and in (E) and (F) XPS spectra of the Si-2p and Al-2p peaks.

deposited, and the film seems to be homogeneous. The Al and Si may therefore not yet have separated into clusters, or the clusters are yet too small to be detected. However, after 50 s of sputtering, when a 5 nm layer has been deposited, elongated Al nanocrystals with a diameter of 3 nm can be observed (see figure 3(B)). As deposition progresses, the length of the Al nanocrystals increase as the layer thickness increases and reach a diameter of 5 nm. The core loss EELS results in figure 4(B), from the area in figure 4(A), show that not all Al has been precipitated into Al clusters, i.e., some still remains in the aSi matrix.

The nanowires are distributed spatially in the aSi with an aSi wall-size of about 2 nm and a uniform Al nanowire diameter of about 5 nm, as shown in the cross-sectional TEM image in figure 5(A) and the EFTEM image of Al in figure 5(B). Figure 5(A) shows that an aSi layer is present between the aSi/Al film and the Si-substrate, thus, the nanowires do not seem to nucleate directly on the crystalline Si substrate. This is in agreement with the initial stages of

deposition shown in figure 3. Figure 5(C) shows the corresponding fast Fourier transform image, with diffraction spots from several Al nanowire orientations. The nanowires seem thus not to have a preferred orientation relationship with the substrate. The Al nanowires in the $Si_{0.6}Al_{0.4}$ sample are crystalline, but are not mono-crystalline along the length of the wire. The nanowires does not grow in the same orientation. It is a clear compositional segregation between Si and Al, this can be seen thom the EDS map in figure 5(D). Figures 5(E) and (F) presents XPS spectra of the Si-2p and Al-2p peak of sample $Si_{0.6}Al_{0.4}$. The Si-2p spectrum shows two peaks corresponding to the spin–orbit coupled $Si_{3/2}^0$ and $Si_{1/2}^0$ peak from aSi. The Al-2p peak shows the spin–orbit coupled peaks from crystalline Al, in addition to some Al-oxide peaks. The XPS spectra shows clearly the oxidation state of Si and Al, elemental amorphous Si and crystalline Al, which is different from what has previously been found for mixed SiAl. [26] During sputtering, some Ar (0.002 at%) have been incorporated into the film. This have been measured with Rutherford backscattering
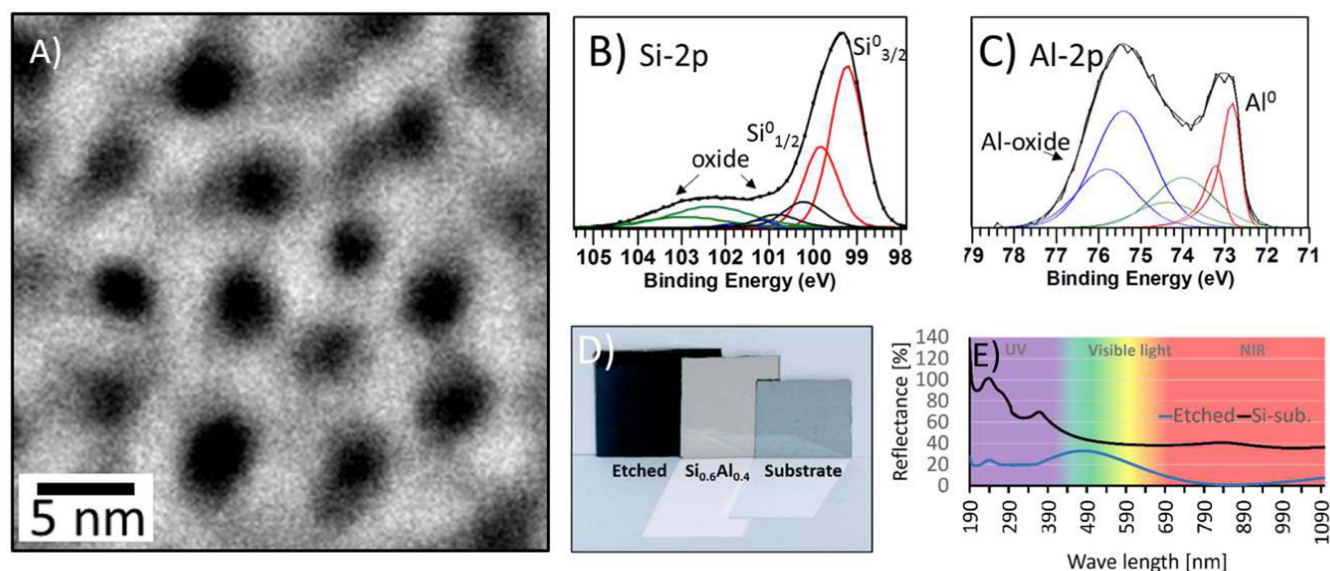
Figure 6. Results from the etched $Si_{0.6}Al_{0.4}$ sample. (A) HAADF plane view image. (B) Si-2p XPS spectrum. (C) Al-2p XPS spectrum. (D) Photo of a Si substrate, $Si_{0.6}Al_{0.4}$, and the etched sample, showing a change in color after etching. (E) Reflectance from the etched sample compared to a Si substrate.

spectroscopy and XPS. The Ar content is mainly found connected to the Al nanowires.

Nanoporous structures of aSi were made by removing the Al nanowires, see figure 1(III). This was achieved using a 20% diluted HCl solution for 10–12 hours, which removed Al without etching the aSi matrix. The top part of figure 1(III) shows a sketch of the structure without the Al, and the bottom part a TEM image of the real processed sample. Figure 1(III) demonstrates that the removal of the Al nanowires has resulted in the creation of a nanoporous structure containing nanotunnels, with the same dimensions and morphology as the nanowires. A high angle annular dark field (HAADF) STEM image of the top (plane view image) of the etched structure can be seen in figure 6(A). XPS measurements in figures 6(B) and (C) shows presence of less than 5 at% Al after etching. The remaining Al in the Si nanostructures after etching is a mixture of pure Al and Al-oxide.

After etching the Al nanowires, the remaining nanoporous aSi surface turns dark, see figure 6(D). This can also be seen from the reflectance spectra in the region of Si absorption (below 1200 nm) in figure 6(E). For low wavelengths (UV light at 190 nm) the reflectance has dropped from 65% down to only 20%.

The unique structure of these materials makes them interesting for many applications. Typical examples include: (a) magnetic media sensors [31], for which the nanoholes in the etched samples can be filled with a material such as CoPt, (b) thermoelectric devices [32], where the unetched films could be deposited on a high dielectric substrate, (c) solar cell structures [33] where the unetched sample could work as a localized back-contact, while the etched samples as an anti-reflection coating. Moreover, by etching the sample and crystallizing the aSi, the material system could be incorporated into a hetero-junction solar cell structure.

4. Conclusion

In this paper we have shown that we have developed a novel, inexpensive low temperature route for creating crystalline Al nanowires embedded in an aSi matrix, based on the immiscibility between Si and Al. Introducing these nanowires into photovoltaic applications, energy storage devices, and thermoelectric materials, may have new technological consequences. The main results of this paper are:

1. We have made Al nanowires in aSi by co-sputtering Al and Si from two targets at room temperature.
2. Changing the Al–Si stoichiometry results in other Al structures, such as Al nanoparticles (at 30 at% Al).
3. The Al nanowires do not extend from the Si substrate surface, but a thin aSi layer is present at the interface.
4. The initiation process starts with the growth of small Al nanocrystals in an Al-rich aSi layer.
5. By etching away the Al we observed a reduced reflectance. However, some Al still remain in the tunnels as pure Al and Al-oxide.

ORCID iDs

Annett Thøgersen ⬤ https://orcid.org/0000-0002-4064-1887

References

[1] Selj J H, Marstein E M, Thøgersen A and Foss S-E 2011 *Phys. Status Solidi* c **8** 1860

[2] Jia G, Eisenhawer B, Dellith J, Falk F, Thøgersen A and Ulyashin A 2013 *J. Phys. Chem.* C **117** 1091

[3] Park N-M, Choi C-J, Seong T-Y and Park S-J 2001 *Phys. Rev. Lett.* **86** 1355

[4] Barbagiovanni E G, Lockwood D J, Simpson P J and Goncharova L V 2014 *Appl. Phys. Rev.* **1** 011302

[5] Tian B, Zheng X, Kempa T J, Fang Y, Yu N, Yu G, Huang J and Lieber C M 2007 *Nature* **449** 885

[6] Tsakalakos L, Balch J, Fronheiser J, Korevaar B A, Sulima O and Rand J 2007 *Appl. Phys. Lett.* **91** 233117

[7] Zgirski M, Riikonen K-P, Touboltsev V and Arutyunov K 2005 *Nano Lett.* **5** 1029

[8] Benson J, Boukhalf S, Magasinski A, Kvit A, Yushin G and Nano A C S 2012 *ACS Nano* **6** 118–25

[9] Au M, McWhorter S, Ajo H, Adams T, Zhao Y and Gibbs J 2010 *J. Power Sources* **195** 3333

[10] Banerjee P, Perez I, Henn-Lecordier L, Lee S B and Rubloff G W 2009 *Nat. Nanotechnol.* **4** 292

[11] Boukai A I, Bunimovich Y, Tahir-Kheli J, Yu J-K, Goddard W A III and Heath J R 2008 *Nature* **451** 168

[12] Zhao Y S, an Di C, Yang W, Liu G Y Y and Yao J 2006 *Adv. Funct. Mater.* **16** 1985

[13] Duan X, Huang Y, Cui Y, Wang J and Lieber C M 2001 *Nature* **409** 66

[14] Martensson T, Carlberg C, Borgstrom P, Montelius M, Seifert W and Samuelson L 2004 *Nano Lett.* **4** 699

[15] Zaremba-Tymieniecki M, Li C, Fobelets K and Durrani Z A K 2010 *IEEE Electron Device Lett.* **31** 860

[16] Woodruff J H, Ratchford J B, Goldthorpe I A, McIntyre P C and Chidsey C E D 2007 *Nano Lett.* **7** 1637

[17] Mahenderkar N K, Liu Y-C, Koza J A and Switzer J A 2014 *ACS Nano* **8** 9524

[18] Jensen I J T, Diplas S and Løvvik O M 2010 *Phys. Rev.* B **82** 174121

[19] Liang S-M and Schmid-Fetzer R 2014 *Acta Mater.* **72** 41

[20] Murray J L and McAlister A J 1984 *Bull. Alloy Phase Diagr.* **5** 74

[21] Fukutani K, Tanji K, Motoi T and Den T 2004 *Adv. Mater.* **16** 1456

[22] Fukutani K, Ishida Y, Aiba T, Miyata H and Den T 2005 *Appl. Phys. Lett.* **87** 253112

[23] Fukutani K, Tanji K, Saito T and Den T 2005 *J. Appl. Phys.* **98** 033507

[24] Fukutani K, Ishida Y, Tanji K and Den T 2007 *Thin Solid Films* **515** 4629

[25] Adams C D, Srolovitzand D J and Atzmon M 1993 *J. Appl. Phys.* **74** 1707

[26] Thoegersen A, Stange M, Jensen I J T, Røyset A, Ulyashinand A and Diplas S 2016 *APL Mater.* **4** 036103

[27] Kailun W, Zuli L and Kailun Y 1999 *Vacuum* **52** 435

[28] Tan X, Zhou Y C and Zheng X J 2005 *Surf. Coat. Technol.* **197** 288

[29] Kurokawa Y, Kato S, Watanabe Y, Yamada A, Konagai M, Ohta Y, Niwa Y and Hirota M 2012 *Jpn. J. Appl. Phys.* **51** 11PE12

[30] Kanematsu D, Yata S, Terakawa A, Tanaka M and Konagai M 2015 *Japan. J. Appl. Phys.* **54** 102301

[31] Yasui N, Imada A and Den T 2003 *Appl. Phys. Lett.* **83** 3347

[32] Hicks L D and Dresselhaus M S 1993 *Phys. Rev.* B **47** 16631

[33] Cui Y, Wei Q, Park H and Lieber C M 2001 *Science* **293** 1289